ACS APPLIED MATERIALS & INTERFACES

Research Article

Cite This: ACS Appl. Mater. Interfaces XXXX, XXX, XXX−XXX

www.acsami.org

Glutathione-Capped Ag_2S Nanoclusters Inhibit Coronavirus Proliferation through Blockage of Viral RNA Synthesis and Budding

Ting Du,[†] Jiangong Liang,[†] Nan Dong,[‡] Jian Lu,[†] Yiying Fu,[†] Liurong Fang,[‡] Shaobo Xiao,*[,‡] and Heyou Han*[,†]

[†]State Key Laboratory of Agricultural Microbiology, College of Food Science and Technology, College of Science, and [‡]State Key Laboratory of Agricultural Microbiology, College of Veterinary Medicine, Huazhong Agricultural University, Wuhan 430070, P. R. China

Supporting Information

ABSTRACT: Development of novel antiviral reagents is of great importance for the control of virus spread. Here, Ag_2S nanoclusters (NCs) were proved for the first time to possess highly efficient antiviral activity by using porcine epidemic diarrhea virus (PEDV) as a model of coronavirus. Analyses of virus titers showed that Ag_2S NCs significantly suppressed the infection of PEDV by about 3 orders of magnitude at the noncytotoxic concentration at 12 h postinfection, which was further confirmed by the expression of viral proteins. Mechanism investigations indicated that Ag_2S NCs treatment inhibits the synthesis of viral negative-strand RNA and viral budding. Ag_2S NCs treatment was also found to positively regulate the generation of IFN-stimulating genes (ISGs) and the expression of proinflammation cytokines, which might prevent PEDV infection. This study suggest the novel underlying of Ag_2S NCs as a promising therapeutic drug for coronavirus.

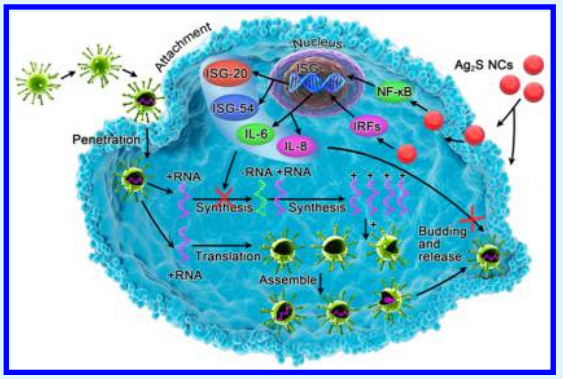

KEYWORDS: *Ag_2S nanoclusters, antiviral, replication, IFN-stimulating genes, proinflammation cytokines*

1. INTRODUCTION

Nanoparticles have shown great potential advantages in antiviral activity. Up to now, several kinds of nanoparticles have been reported to exhibit antiviral activity to a certain extent, such as silver nanoparticles,[1−3] functional gold nanoparticles,[4,5] carbon-based nanomaterials,[6−10] polyoxometalate,[11,12] nanoclay,[13] and silicon nanoparticles.[14] Generally, aiming the early stages of viral absorption and entry was the most universal tactic in the course of development of antiviral therapies.[15−17] Like other biological interactions, the properties of the nanostructures allow them to adapt well to competing with these recognition sites to inhibit viral entry into cells.[18,19] However, there were several common drawbacks for the previously reported antiviral materials. For instance, the widely used strategy was based on blocking viral attachment or viral entry into cells, and the nanoparticles have no suppressive effect of on the progeny of the virus in the late viral replication.[20,21] Therefore, more efforts should be made to develop safe, high-performance antiviral drugs targeting different stages of virus infectious life cycle.

Coronavirus is a life threatening virus that could lead to serious respiratory tract infectious diseases in humans. Porcine epidemic diarrhea virus (PEDV), a positive-strand RNA virus, membering of the family *Coronaviridae* and genus *Alphacoronavirus*, is a vital animal virus model for the study of coronavirus. As a serious, highly epidemical and ruinous intestinal disease, PEDV has brought tremendous financial loss in the global swine industry, especially in China, Korea, Japan, and Thailand, since it was first found in piglets and fattening swine in Europe.[22,23] Unfortunately, the control of PEDV was primarily dependent on vaccination in advance, suggesting the necessity of developing novel antiviral drugs.

Ag_2S nanocrystals, also called quantum dots (QDs), are a class of ideal narrow-band-gap NIR fluorescent materials[24] and have been used in optical and electronic devices, biolabeling, and bioimaging due to their advantages of low or no toxicity to living tissues, good chemical stability, and outstanding optical limiting properties.[25,26] Wan's group has reported that NO can be released by glutathione (GSH)-stabilized Ag_2S QDs conjugated with RSNOs under certain light irradiation with the function of NIR fluorescence imaging.[27] Achilefu's group has successfully conjugated a tumor-avid peptide to Ag_2S QDs that can be selectively delivered to tumor cells and tissue.[28] Chen's group has shown that Ag_2S nanocrystals can be used as photothermal therapy agents *in vitro* and *in vivo*.[29] Meng's group has proposed a DNA logic gate platform to enable the realization of femtomolar level miRNA analysis through NIR Ag_2S nanocrystals for their autofluorescence properties.[30] To our knowledge, there is still no report available about the function of Ag_2S NCs as an antiviral agent.

Received: September 11, 2017
Accepted: January 16, 2018
Published: January 16, 2018

DOI: 10.1021/acsami.7b13811
ACS Appl. Mater. Interfaces XXXX, XXX, XXX−XXX

Scheme 1. Possible Mechanisms of the Antiviral Activity of Ag_2S NCs[a]

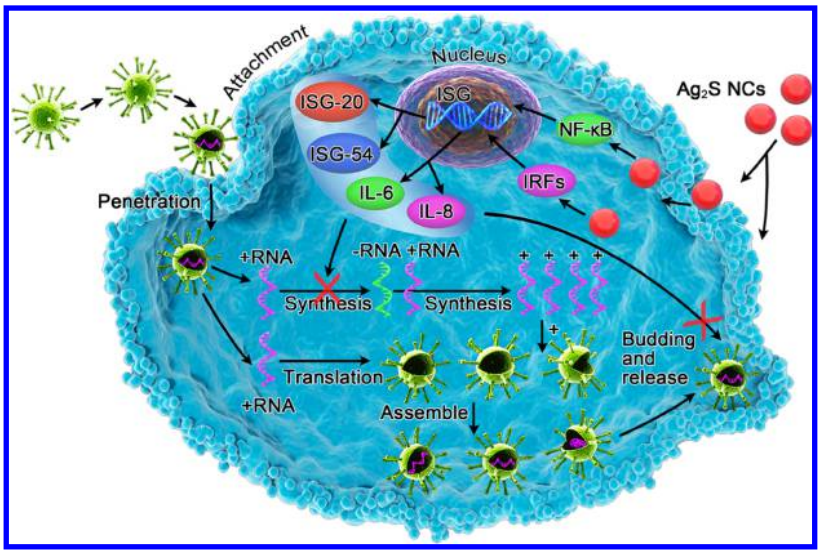

[a]The replication cycle of viruses consists of the four consecutive steps of attachment, penetration, replication and budding. The study of underlying molecular mechanisms indicated that Ag_2S NCs treatment inhibits the synthesis of viral negative-strand RNA and viral budding. Meanwhile, the production of ISGs and the upregulation of proinflammatory cytokines might have a crucial role in the inhibitory effect of Ag_2S NCs.

Here, we report the use of Ag_2S NCs for viral inhibition (Scheme 1). Assays *in vitro* showed that cells treated with Ag_2S NCs restrained the propagation of PEDV possibly through inhibiting the synthesis of viral negative-strand RNA and viral budding. In addition, the antiviral activity of the Ag_2S NCs also might be attributed to the activation of ISG proteins and proinflammatory cytokines.

2. EXPERIMENTAL SECTION

2.1. Synthesis of Ag_2S NCs. In this work, the synthesis of glutathione (GSH)-capped Ag_2S NCs was based on the previous literature.[31] Selecting the suitable capping reagent is the key to the preparation of tunable Ag_2S NCs. GSH is a small molecule peptide that consists of three amino acids and can serve as a vital scaffold to prevent the growth of large nanoparticles. In addition, GSH contains multiple functional groups, indicating that the resulting GSH-capped Ag_2S NCs will have good water solubility. For synthesis of Ag_2S NCs, 0.160 g of sulfur was added to 10.0 mL of hydrazine hydrate ($N_2H_4{\cdot}H_2O$) and stirred at ambient temperature to thoroughly dissolve. After sedimentating for 48 h at 4 °C, the resulting aqueous S^{2-} source was diluted 20 times before further use as the S^{2-} source, and then supramolecular hydrogel was formed by mixing GSH and Ag^+ ($AgNO_3$ as the Ag^+ source) in a fixed molar ratio in N_2 atmosphere. Next, 4.0 mL of S^{2-} source solution was injected and stirred constantly for 30 min. The obtained Ag_2S NCs were purified by adding isopropanol, followed by centrifuging the mixture. Finally, the precipitate was redispersed in ultrapure water and kept at 4 °C for future use. GSH-capped Ag_2S NCs with a different FL wavelength were synthesized through changing the amount GSH and the proportion of Ag^+ to $S{-}N_2H_4{\cdot}H_2O$.

2.2. Cell Viability. Vero cells were cultured in the 96-well plates until approximately 80−90% confluence; the cells were exposed with different concentrations (23, 46, and 92 μg/mL) of Ag_2S NCs and GSH (10 mM). Cells treated with the DMEM (2% FBS) were used as control. After culturing the cells for 24 and 48 h, the supernatant was superseded by 100 μL of DMEM (2% FBS) and 20 μL of MTT reagent (5 mg/mL). Through further 4 h of incubation, 150 μL of dimethyl sulfoxide (DMSO) solution was supplemented after the medium was discarded. The OD value at 570 nm was measured.

2.3. One-Step Growth Curves. The 80−90% confluence Vero cells were incubated with control DMEM (containing 10 μg/mL trypsin) or Ag_2S NCs at 37 °C for 2 h. Subsequently, the Vero cells were treated with PEDV at 37 °C at a multiplicity of infection (MOI) of 0.01. After 1 h infection, the inoculums were discarded, and then the cell monolayers were cultured separately in control DMEM (containing 10 μg/mL trypsin) or Ag_2S NCs at 37 °C for 1, 3, 6, 9, 12, 24, 36, 48, 60, and 72 h postinfection (hpi). After three freeze−thaw cycles, removal of cell debris by centrifuging the cells at 4 °C. The average titers of all samples were measured via plaque assay.[32,33]

2.4. Plaque Assays. The plaque assays of PEDV were performed according to the previously reported with minor modifications.[34] In brief, Vero cells were inoculated and incubated in DMEM (10% FBS) in a 6-well plate until 90−100% confluence, followed by infection with 10-fold dilutions (800 μL/well) of PEDV-containing inoculum to allow virus infection for 1 h. Then the cell monolayers were coated with Bacto agarose and 2 × DMEM in a fixed volume ratio of 1:1 (including 10 μg/mL trypsin). At 2−3 days postinfection, the plaques were counted. Through three independent experiments, the standard deviations and average plaque number were calculated. All the virus titers were dispalyed as plaque forming units (PFU)/mL.

2.5. Indirect Immunofluorescence. Vero cells were cultured to approximately 70−80% confluenc and , then unexposed or exposed with Ag_2S NCs for 2 h, followed by washing twice with PBS and infection with PEDV at 0.01 MOI. After 1 h of incubation, free viruses were removed through extensive rinsing, and the Vero cells were incubated with control DMEM (containing 10 μg/mL trypsin) or Ag_2S NCs for 12 h. Next, the fixation of cells was performed with cold 4% paraformaldehyde for 15 min, and the permeabilization was carried out with methanol (−20 °C) at the ambient temperature. Next, the PEDV-infected Vero cells were blocked by 5% (w/v) BSA for 45 min and then measured with a mouse monoclonal antibody against the PEDV N protein and FITC-conjugated goat anti-mouse IgG antibody (Invitrogen). Subsequently, cells nucleus were counterstained with DAPI. After three washes, the photographs were obtained by an Olympus IX73 microscope.

2.6. Western Blot. Vero cells were unexposed or exposed with Ag_2S NCs for 2 h, followed by infection with 0.05 MOI PEDV. After 1 h of infection, the cell monolayers were incubated with control DMEM (containing 10 μg/mL trypsin) and Ag_2S NCs for 12 h and then harvested by adding 150 μL of lysis buffer. After boiling the whole cell extracts in SDS protein sample buffer, equivalent samples were performed with 12% SDS−polyacrylamide gel electrophoresis, and then the expression of the PEDV N protein was determined. The expression of β-actin was investigated to represent a same amount of protein sample loading.

DOI: 10.1021/acsami.7b13811
ACS Appl. Mater. Interfaces XXXX, XXX, XXX−XXX

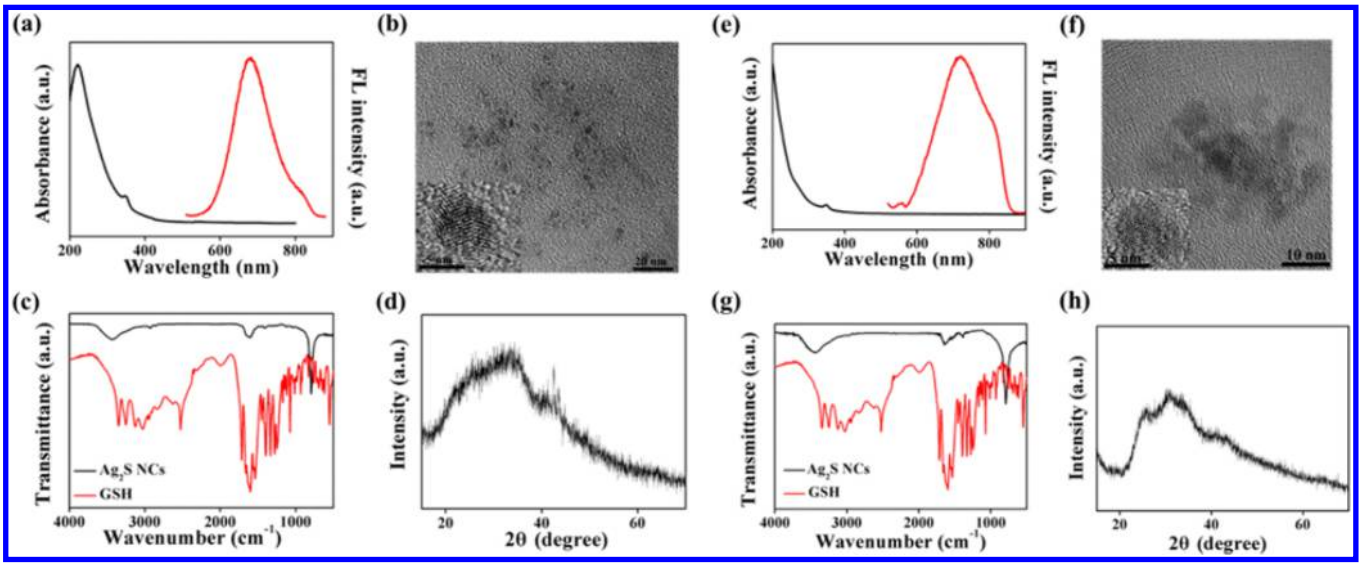

Figure 1. (a, e) UV−vis and fluorescence spectrum of GSH-capped Ag_2S NCs (681 and 722 nm). (b, f) The TEM and HRTEM images of GSH-capped Ag_2S NCs (681 and 722 nm). (c, g) The FT-IR spectra of resultant GSH-capped Ag_2S NCs (681 and 722 nm) and GSH. (d, h) XRD patterns of resultant GSH-capped Ag_2S NCs (681 and 722 nm).

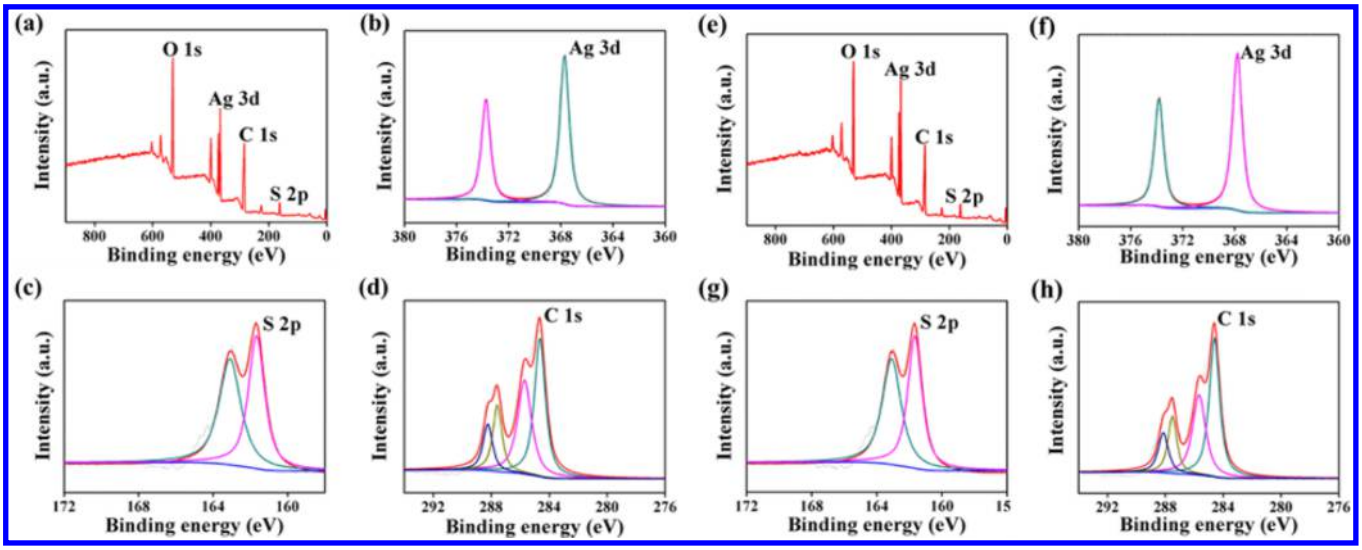

Figure 2. (a, e) XPS spectra of GSH-capped Ag_2S NCs (681 and 722 nm). High-resolution XPS spectra of Ag 3d (b, f), S 2p (c, g), and C 1s (d, h) of the Ag_2S NCs.

2.7. Influence of Ag^+ and S^{2-} on Viral Replication. To measure the effect of the release of Ag^+ from Ag_2S NCs on viral replication, Vero cells were unexposed or exposed with different concentrations of Ag^+ (or S^{2-}) at 37 °C. Next, Vero cells were treated with PEDV at 0.01 MOI. After 1 h of infection, the cells were extensively rinsed to clear the free viruses and then treated with control DMEM (containing 10 μg/mL trypsin) or different concentrations of Ag^+ (or S^{2-}) for 24 hpi. The remaining steps are consistent with indirect immunofluorescence assays.

Furthermore, the effect of Ag^+ (or S^{2-}) on viral replication was quantitatively verified by measuring virus titer. Briefly, after mock treatment or treatment with various concentrations of Ag^+ (or S^{2-}), the cells were then treated with PEDV. After 1 h of infection, cells were rinsed with PBS and incubation with control DMEM or Ag^+ (or S^{2-}) for 24 h. Finally, the cells were harvested and stored in ultralow-temperature refrigerator. The average titers of all samples were calculated through plaque assays.

2.8. Attachment Assay. The 90−100% confluent Vero cells were prechilled at 4 °C for 30 min. PEDV samples containing different concentrations of Ag_2S NCs were added into 6-well plates and cultured at 4 °C to permit virus attachment. After 2 h of incubation, the attachment was stopped by two washes of the cells with ice-cold PBS. Finally, cells were coated with Bacto agarose and 2 × DMEM in a fixed volume ratio of 1:1 (supplemented with 10 μg/mL trypsin). The titer of PEDV was investigated by plaque assay.[35]

2.9. Penetration Assay. After washing Vero cells with PBS, a PEDV inoculum (800 μL/well) was permitted to adhere to the cells for 2 h at 4 °C. Then the supernatant was discarded, followed by two washes of the cells with PBS and addition of the mediums containing different concentrations of Ag_2S NCs; the cells were cultured for an additional 3 h to initiate viral penetration (37 °C/5% CO_2). Next, nonpenetrated virions were discarded by rinsing the cell monolayer twice with PBS, and then the overlay inoculum was added. The remaining steps were similar to those for attachment assay.[36]

2.10. Viral Negative-Strand RNA Replication. After 2 h mock treatment or treatment with Ag_2S NCs, the Vero cells were treated with PEDV for 1 h, followed by incubating separately with DMEM (containing 10 μg/mL trypsin) or Ag_2S NCs for 4, 5, 6, and 7 at 37 °C/5% CO_2. Total RNA was extracted and quantified by RT-PCR.

2.11. Release Analysis. Vero cells were infected with PEDV at 0.01 MOI for 1 h (37 °C/5% CO_2). Afterward, the infected cells were

DOI: 10.1021/acsami.7b13811
ACS Appl. Mater. Interfaces XXXX, XXX, XXX−XXX

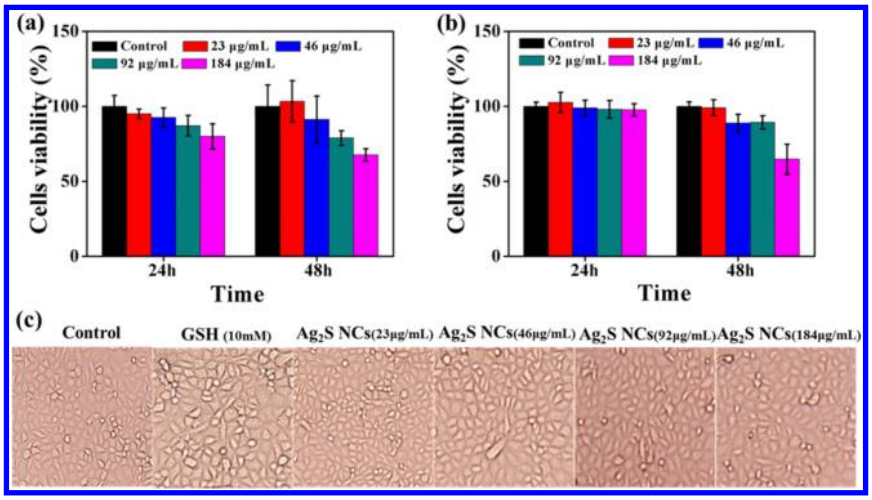

Figure 3. Cytotoxicity of different concentrations of Ag_2S NCs (681 nm) by MTT (a) and CCK-8 (b) assay. (c) Vero cell morphology after incubation with different concentrations of Ag_2S NCs (23−184 μg/mL) and 10 mM GSH.

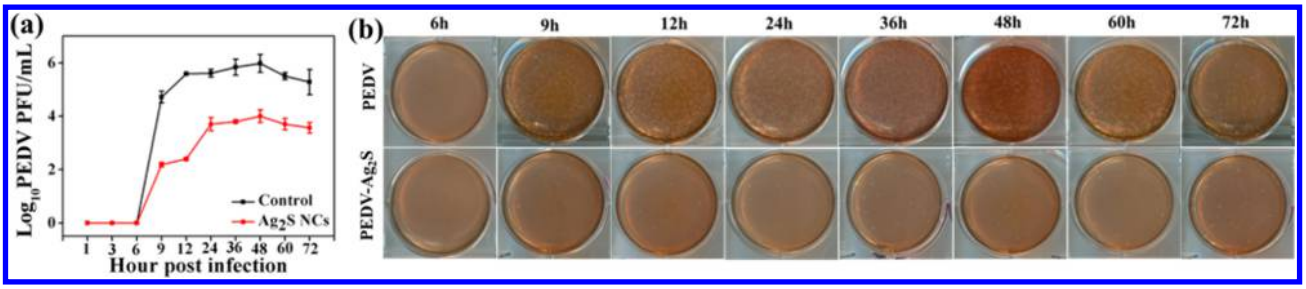

Figure 4. Growth curves of viruses after treatment or untreatment with Ag_2S NCs. Cells were infected with PEDV for the indicated periods of time (a). Plaque-reduction assay after neutral red staining. Pictures were taken 2−3 days following infection (b). Each data point represents mean ± SD (N = 3).

cultured in a 5% CO_2 incubator for indicated infection periods of time, followed by mock-treatment or treatment with Ag_2S NCs at 37 °C for 15, 30, 45, and 60 min. Next, the supernatant and cell lysate were harvested and stored at −80 °C, respectively. Each sample was determined by plaque assay in triplicate.[37]

2.12. Statistical Analysis. The experimental data was analyzed by an independent t test. Statistical significance was decided with a $^*p < 0.05$ and $^{**}p < 0.01$. Each data point represents mean ± SD (N = 3).

3. RESULTS

3.1. Characterization of Ag_2S NCs. The optical properties, morphology, and chemical structure of the as-prepared Ag_2S NCs are shown in Figure 1. The maximum emission wavelength of Ag_2S NCs at 681 and 722 nm with excitation at 450 nm exhibited a red light emission. As shown in Figures 1a and 1e, no typical absorption band of Ag nanoparticles or Ag (0) NCs were observed, indicating that Ag_2S NCs rather than nanocrystals were formed at room temperature.[31] This result was further verified by measuring the powder X-ray diffraction (XRD) of Ag_2S NCs, and no distinct crystallinity was found (Figures 1d and 1h), which well supported the result of UV−vis absorption spectra. Figures 1b and 1f show the characteristic TEM images of the resultant Ag_2S NCs. It could be observed that these Ag_2S NCs (681 and 722 nm) were spherical and greatly dispersible, and the average diameters were about 2.5 ± 0.6 and 4.1 ± 1.5 nm, respectively. Figure S1a presents the hydrodynamic size distribution of Ag_2S NCs (681 nm); the average size was 3.7 nm, which was determined by dynamic light scattering (DLS). Figure S1b shows that the average size of Ag_2S NCs (722 nm) was 5.3 nm.

To further understand the characteristics of the as-prepared Ag_2S NCs, the surface functional groups and valence status of the Ag_2S NCs were performed. As shown in Figure 1c (681 nm) and Figure 1g (722 nm), the Ag_2S NCs displayed a typical peak at 3000−3500 and 785 cm^{-1}, ascribing to the stretching vibration of O−H (or N−H) and C−H. The peak around 1665 cm^{-1} was attributed to the C═O vibration of the carboxylic acid groups on the surface of Ag_2S NCs. At 2490 cm^{-1}, no apparent absorption peak for the free thiol group was observed at the same position, indicating that GSH molecules were connected with the surface of Ag_2S NCs through Ag−thiol bonds. The full range XPS analysis (Figures 2a and 2e) of the resultant Ag_2S sample clearly showed four evident peaks at 163.1, 287.6, 367.7, and 531.6 eV, corresponding to S 2p, C 1s, Ag 3d, and O 1s. A XPS spectrum of Ag 3d (Figures 2b and 2f) confirmed the presence of Ag(0) (367.7 eV). This revealed that Ag ions exist in the form of monovalent in Ag_2S NCs. The S 2p peaks at 163.1 and 161.7 eV were ascribed to S and Ag−S, respectively (Figures 2c and 2g).[38] The four fitted peaks at 284.6, 285.7, 287.6, and 288.2 eV in the C 1s spectrum were assigned to $-CH_2-CH_3$, −CH−, $-CONH_2$, and −COOH groups, respectively (Figures 2d and 2h). The surface components of the Ag_2S NCs acquired by the XPS were in consistent with FT-IR results.

3.2. Toxicity of Ag_2S NCs on Vero Cells. The cytotoxicity of Ag_2S NCs on Vero cells was evaluated by determining cellular viability using an MTT and CCK-8 assay (Figure 3 and Figure S2). The viability of cells treated by Ag_2S NCs (681 nm), or GSH was measured at a concentration range of 23−184 μg/mL. As shown in Figures 3a and 3b, after cultivation for 24 and 48 h, the effect of 46 μg/mL Ag_2S NCs on cell viability was inappreciable, and the survival rate of Vero cells was over 90%. Meanwhile, the cell morphology was not influenced at this concentration (Figure

DOI: 10.1021/acsami.7b13811
ACS Appl. Mater. Interfaces XXXX, XXX, XXX−XXX

3c). When the concentration reached 184 μg/mL, the cytotoxicity of Ag_2S NCs was relatively low, and the survival rate of Vero cells was about 68% after 48 h incubation. Gui et al. reported the cell viability far exceeded 91% after treatment with QDs for 48 h, at a Ag_2S QDs exposure concentration of 1.0 mg/mL, which was similar to our present study.[25] Hence, 46 μg/mL was applied for the subsequent tests.

3.3. Influence of Ag_2S NCs on PEDV Replication. One-step growth curve was plotted to detect the PEDV titer after treatment with 46 μg/mL Ag_2S NCs to evaluate the effect of Ag_2S NCs on PEDV replication. In Figure 4a, compared to the negative control group, significant viral titer inhibition was observed in cells treated with Ag_2S NCs. When treated with Ag_2S NCs at 12 hpi, the plaque formation unit (PFU) was significantly decreased from 3.8×10^5 to 2.5×10^2 PFU/mL as shown by the results from Figure 4b. Therefore, the number of plaques and the titer of virus verified that Ag_2S NCs indeed possesses excellent antiviral activity against viral replication.

PEDV nucleocapsid (N), the RNA-binding protein, acts a vital role in the viral life cycle and can serve as a target for precise and early diagnosis of PEDV infection.[39] To validate the inhibitory effect of Ag_2S NCs on the proliferation of PEDV, the expression level of PEDV N protein was detected. Briefly, the infected cells were incubated with different concentrations of Ag_2S NCs or control DMEM (including 10 μg/mL trypsin). After 12 hpi, the cells treated with Ag_2S NCs at different concentrations showed an obvious difference in the number of infected cells (indicated via green fluorescence) compared to the untreated PEDV-infected group (Figure 5). This indicated that the expression of PEDV N protein was continuously downregulated in a concentration-dependent manner, which was consistent with the growth curves of virus.

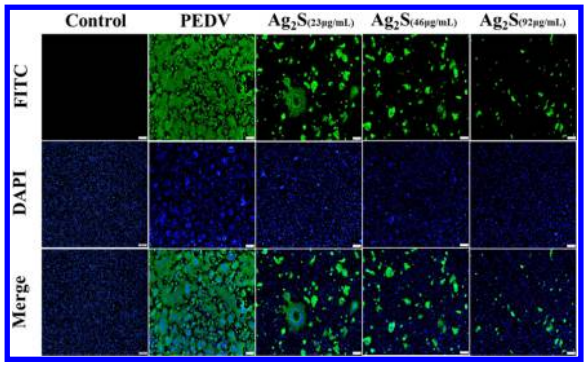

Figure 5. Indirect immunofluorescence assay of PEDV-infected Vero cells after treatment or untreatment with different concentrations of Ag_2S NCs. Scale bar: 100 μm.

3.4. Effect of Ag_2S NC Size on the Multiplication of PEDV. As is well-known to all, the size of nanoparticles plays an indispensable role in their interactions with external systems.[40,41] To further characterize the potential influence of the size on the multiplication of PEDV, we tested the interaction of Ag_2S NCs-681 (Ag_2S NCs-S) and Ag_2S NCs-722 (Ag_2S NCs-L) with PEDV by a plaque formation assay. As shown in Figure 6b, when compared to untreated cells, the virus titer in the cells treated with Ag_2S NCs-S and Ag_2S NCs-L was significantly reduced by 2.4 log and 3.0 log, respectively, and this result is more intuitively shown in Figure S3. To further illustrate the differences of viral multiplication at the protein level, the expression of PEDV N protein after treatment with Ag_2S NCs-S and Ag_2S NCs-L was measured by indirect immunofluorescence assay and Western blot assay. The green fluorescence signal of the group exposed with Ag_2S NCs-S or Ag_2S NCs-L was obviously reduced compared with the control, and the Ag_2S NCs-S-treated group had a more pronounced decrease tendency than the Ag_2S NCs-L-treated group (Figure 6a). The Western blot assay indicated that the number of PEDV N protein expression was significantly downregulated compared with that of the control after treatment with Ag_2S NCs-S or Ag_2S NCs-L (Figure 6c). The overall results indicated that Ag_2S NCs-S-treated group had a pronounced inhibition on PEDV infection and excluded the possibility that the aforementioned plaque reductions were arised from cytotoxicity of the Ag_2S NCs. Interestingly, the results were similar to those reported by our group about the effects of different sizes of CdTe quantum dots on pseudorabies virus.[42] In general, smaller nanoparticles cause weaker hydrodynamic and shear force when they entry into the cell, which make them penetrate deeper than the larger nanoparticles.[41,43,44] This may be the reason that lead to a better antiviral effect of small size Ag_2S NCs.

3.5. Effect of Ag^+ and S^{2-} on the Multiplication of PEDV. To probe the effect of release of Ag^+ from Ag_2S NCs on viral replication, infected cells were exposed with various concentrations of Ag^+. After incubation of 24 hpi, the results showed that 4.8 ± 1.3 μM Ag^+ was released when PEDV was exposed with 46 μM Ag_2S NCs, which was quantitative detection through Inductively coupled plasma mass spectrometry (ICP-MS). In Figure S4a, green fluorescence signals of the group treated with different concentrations of Ag^+ were not significantly decreased compared with the PEDV-infected control, which was further verified by Figure S4b. In addition, the effects of different concentrations of S^{2-} ($Ksp(Ag_2S) = 6 \times 10^{-50}$) on viral replication were also investigated. From Figures S4c and S4d, it can be seen that the results were similar to the aforementioned ones, suggesting the release of Ag^+ and S^{2-} from Ag_2S NCs cannot play a dominate role in the antiviral ability of Ag_2S NCs.

3.6. Effect of Ag_2S NCs on PEDV Replication Cycle. The replication cycle of viruses consists of the four consecutive steps of attachment, penetration, replication, and budding. To further elucidate the mechanism of Ag_2S NCs to inhibit PEDV infection, we performed a series of tests to recognize which step(s) in the life cycle of the virus was inhibited by Ag_2S NCs.

To test whether Ag_2S NCs could inhibit PEDV binding to cells, the impact of Ag_2S NCs on the attachment was estimated by plaque assay. Briefly, the cells were first exposed with different concentrations of Ag_2S NCs and then infected by 0.03 MOI PEDV at 4 °C for 2 h to allow virus attachment. Infected cells untreated with Ag_2S NCs were used as controls. As shown in Figure 7 and Figure S5, the number of plaques after treatment with Ag_2S NCs was similar to that of the control, suggesting that Ag_2S NCs did not inhibit the viral attachment or the virus in the early infection phase. This result also suggested that before viral entry into the cells, Ag_2S NCs did not significantly inhibit PEDV infection by inactivating PEDV directly.

To investigated whether Ag_2S NCs can inhibit viral penetration, PEDV was incubated with the cells at 4 °C for 2 h to allow the virus to attach to the cell surface, followed by initiation of the penetration process by shifting temperature to 37 °C. In Figure 8, there was no remarkable decrease in PEDV titer with the increase of Ag_2S NCs concentration. Meanwhile, no significant plaque-number difference was detected after treatment or untreatment with Ag_2S NCs (Figure S6), suggesting that

DOI: 10.1021/acsami.7b13811
ACS Appl. Mater. Interfaces XXXX, XXX, XXX−XXX

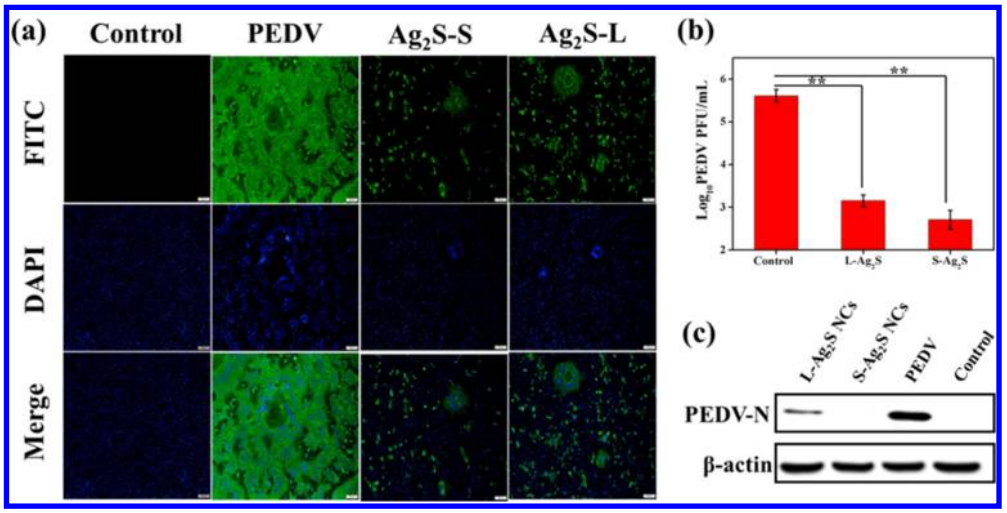

Figure 6. Effect of Ag_2S NCs-S and Ag_2S NCs-L on PEDV. (a) Indirect immunofluorescence assay of PEDV-infected Vero cells after treatment or untreatment with Ag_2S NCs-S and Ag_2S NCs-L. Scale bar: 100 μm. (b) The titer of PEDV in the presence and absence of Ag_2S NCs-S and Ag_2S NCs-L. (c) Detection of PEDV-N protein expression through Western blot assay. The infected cells were exposed with Ag_2S NCs-S and Ag_2S NCs-L for 12 hpi. β-Actin was used as a loading control.

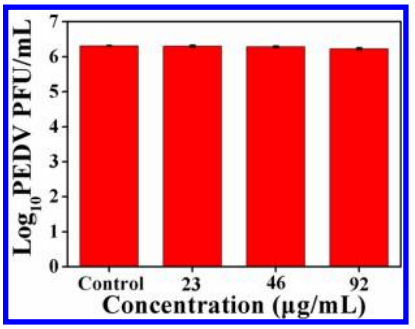

Figure 7. A dose-response study on the relationship between the inhibition efficiency of viral attachment and the amount of Ag_2S NCs.

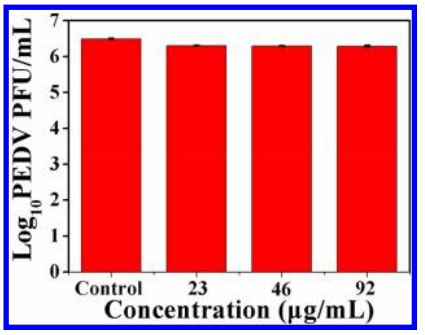

Figure 8. A dose-response study on the relationship between the inhibition efficiency of viral penetration and the amount of Ag_2S NCs.

the Ag_2S NCs had no impact on the process of penetration of the virus on the cell surface. The process of viral entry into host cells involves the recognition between the viral envelope glycoproteins and the cell surface receptors. According to this mechanism, AgNPs modified with mercaptoethanesulfonate can inhibit the virus proliferation by blocking the binding of the virus to cell surface heparin.[45] Owing to the absence of molecules that bind to the virus on the surface of the Ag_2S NCs, the binding of virus to the cell surface receptor cannot be prevented.

To investigate the effects of Ag_2S NCs on the replication step of PEDV, the level of negative-strand RNA of PEDV was tested. Briefly, Vero cells were unexposed or exposed with Ag_2S NCs for 2 h, followed by infecting the cells separately with PEDV for 4, 5, 6, and 7 h. As shown in Figure 9, the synthesis of negative-strand

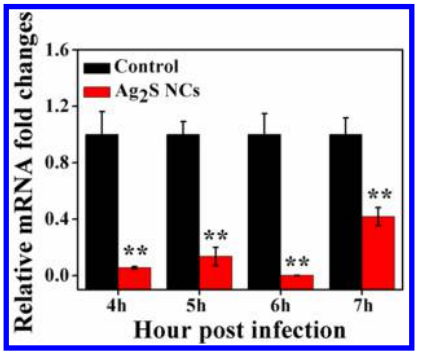

Figure 9. Relative synthesis of negative-strand RNA of PEDV was determined at different hours post infection, with Vero cells mock-treated or treated with Ag_2S NCs.

RNA of PEDV was dramatically downregulated at different hours postinfection compared with the control groups. These results clearly demonstrated the inhibition of Ag_2S NCs on PEDV replication.

The virion nucleocapsids successfully released into the cytoplasm of host cell after viral proteins were synthesized and assembled, and then progeny virions could bud from the plasma membrane on the surface of the infected cell. To determine whether the Ag_2S NCs could influence the virion budding, cells were first treated with PEDV for the indicated time periods and then mock treatment or treatment with Ag_2S NCs for 15, 30, 45, and 60 min. After the infected cells were treated with Ag_2S NCs for different time points, the virus titers in the Ag_2S NCs-treated group were significantly decreased compared with the control groups (Figure 10). This indicated that even if the cells have been infected with PEDV, the subsequent Ag_2S NCs treatment was still effective in inhibiting viral budding.

3.7. Ag_2S NCs Activate Antiviral Innate Immunity. To further probe the potential mechanism of Ag_2S NCs inhibition of PEDV infection, we estimated the impact of Ag_2S NCs on the immune and inflammation response of the host interferon. As previously reported, type I interferons (IFNs) and IFN-

DOI: 10.1021/acsami.7b13811
ACS Appl. Mater. Interfaces XXXX, XXX, XXX−XXX

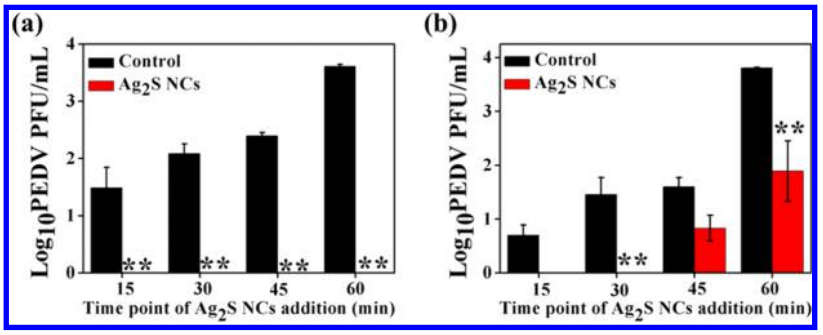

Figure 10. Quantification of the titer of PEDV after the treatment of Ag_2S NCs for a different time point. The virus titer of intracellular (a) and supernatant (b).

stimulated genes (ISGs) were the most famous antiviral innate immune molecules.[46,47] The induction of ISGs and proinflammatory cytokines required the coordination and synergy effects of the transcription factors IRF3 and NF-κB. In order to explore whether Ag_2S NCs promoted the production of IRF-3 and NF-κB, cells were cotransfected with the IRF3-Luc and NF-κB-Luc luciferase reporter plasmids along with the internal control plasmid pRL-TK after unexposure or exposure with Ag_2S NCs. As displayed in Figure 11, the Ag_2S NCs positively

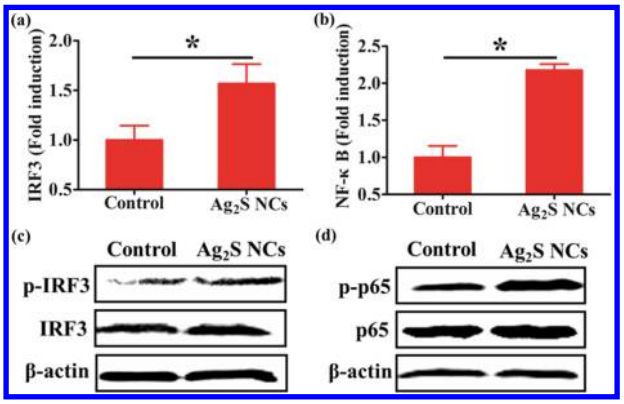

Figure 11. Ag_2S NCs promoted the activation of IRF3 and NF-κB promoter. Vero cells were cotransfected with the IRF3-Luc (a) and NF-κB-Luc (b) along with the pRL-TK plasmid. Luciferase assay was performed after the treatment of Ag_2S NCs for 12 h. (c, d) Ag_2S NCs treatment-induced phosphorylation of IRF3 and p65. Cells were exposed with Ag_2S NCs for 12 h and harvested for Western blot analysis with phosphorylated IRF3 (p-IRF3), IRF3, phosphorylated p65 (p-p65), p65, or β-actin antibodies.

regulated the promoter activity of IRF3 and NF-κB. Meanwhile, production of IRF3 and NF-κB is often marked by the phosphorylation of IRF3 and NF-κB subunit p65, respectively. As expected, when compared with the control, Ag_2S NCs treatment obviously enhanced IRF3 and p65 phosphorylation (Figures 11c and 11d), which were concordant with the findings of the Luciferase tests.

The mRNA expression levels of ISGs and proinflammatory cytokines were determined by real-time RT-PCR. Compared with the control group, the levels of mRNA expression levels of interferon-stimulated genes 20 (ISG-20) and 54 (ISG-54) were increased. Furthermore, the expressions of proinflammatory cytokines were also significantly upregulated after the treatment of Ag_2S NCs, and the mRNA expressions of interleukin 8 (IL-8) and interleukin 6 (IL-6) were 9.3 and 3.3 times higher than that of the untreated controls (Figure 12). It is reported that IL-8

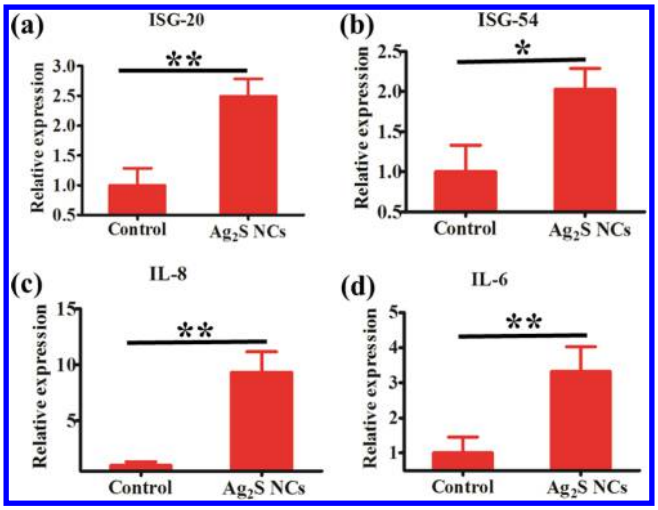

Figure 12. Level of cytokines expression in Vero cells after exposure with 46 μg/mL Ag_2S NCs. The expressions of ISG-20 (a), ISG-54 (b), IL-8 (c), and IL-6 (d) were detected by real-time RT-PCR assay.

upregulation might cause IL-8 recruited neutrophils to phagocytose target antigens, thereby regulating virus replication by triggering Toll-like receptors and activating the IFN-β and ISG.[48] Meanwhile, Yu et al. found that fish TRIM32 could inhibit virus infection by upregulating the interferon immune response, IL-6 and IL-8.[49] It was also reported that ISG-20 could inhibit the synthesis of virus RNA by inhibiting the enzymatic activities.[50] Additionally, ISG-54 was reported to stimulate the expression of phosphorylated STAT1, which would play a crucial part in the immune and inflammatory responses.[51,52] These reports suggested that the production of ISGs and the upregulation of proinflammatory cytokines might have a crucial role in the inhibitory effect of Ag_2S NCs. Yet, the results could not exclude the probability of exploiting other antiviral activity mechanism(s).

4. DISCUSSION

Currently, the antiviral therapies are focused on the following two strategies. First, viral infection starts from the virion adhesion or binding to the host's receptors, followed by penetration and viral replication.[53] So, effective blocking of viral attachment and entry into the cell can have a remarkable prophylactic effect against viral diseases.[54,55] The other strategy is concentrated on inhibition of viral replication and budding (therapeutic effect).[56]

For the antiviral activity, the most widely studied materials include Ag nanoparticles and Au nanoparticles,[57,58] carbon-based materials,[59] silicon nanoparticles,[60] and so on.[61,62] In vitro

DOI: 10.1021/acsami.7b13811
ACS Appl. Mater. Interfaces XXXX, XXX, XXX−XXX

studies have shown that functional AgNPs (or Au nanoparticles) could be acted as drugs against human immunodeficiency virus type 1 (HIV-1),[63] herpes simplex virus type 1(HSV-1),[64] tacaribe virus (TCRV), respiratory syncytial virus (RSV), and so on. Lee et al. constructed the GAG mimetic functionalized silica nanoparticles that can be used as viral entry inhibitors by blocking viral attachment and penetration into cells.[65] Yang et al. reported that functionalized graphene showed highly efficient inhibition on RSV infection by directly inactivating the virus.[66] Zhu's group found that AgNPs@OTV could suppress H1N1 influenza virus infection via ROS-mediated signaling pathways.[67] Furthermore, Yang et al. have shown that AgNPs could inhibit the RSV titers by 2 orders of magnitude based on a tissue culture infectious dose ($TCID_{50}$) assay.[20]

The level of PEDV N protein expression was also checked through Western blot assay after Vero cells were unexposed or exposed with the same concentration of Ag_2S NCs and AgNCs. In Figure S7, Ag_2S NCs showed a stronger inhibitory effect than AgNCs. Moreover, it was reported that DNA-modified gold nanoparticle networks can impede viral attachment and entry into cells for prophylactic effects, and these composite can also produce therapeutic effects.[56] Meanwhile, our previous study proved that CDs can suppress porcine reproductive and respiratory syndrome virus (PRRSV) and pseudorabies virus (PRV) proliferation through activating the prodution of interferon-α production and interferon stimulated genes.[68] Additionally, our previous work also demonstrated that CdTe quantum dots suppress PRV proliferation by altering the structure of viral surface proteins and the leakage of Cd^{2+}.[42] We speculate that nanoparticles with a different composition vary in their antiviral mechanism. To further illustrate the antiviral mechanism of Ag_2S NCs, we investigated the effect of Ag_2Te NPs with a different composition on PEDV by comparing the expression of PEDV N proteins after treatment with various concentrations of Ag_2Te NPs. In Figure S8, Ag_2Te NPs did not exhibit obvious antiviral activity against PEDV, implying that the main antiviral activity of Ag_2S NCs was not dependent on Ag^+.

The antiviral potential of Ag_2S NCs was further evaluated by using another RNA virus, PRRSV (a member of *Arteriviridae*). Consistent with the result for PEDV, Ag_2S NCs also displayed inhibitory effects on the expression level of the PRRSV viral protein (Figure S9). Thus, it can be deduced that Ag_2S NCs might have broad-spectrum antiviral properties against RNA viruses.

5. CONCLUSION

In summary, this study described a one-pot method to prepare hydrosoluble and biocompatible GSH-capped Ag_2S NCs. We demonstrated for the first time that Ag_2S NCs had remarkable antiviral activity against PEDV infection, with the infection inhibited for a 3.0 log reduction in virus titer at the noncytotoxic concentration at 12 hpi. The study of underlying molecular mechanisms indicated that Ag_2S NCs treatment inhibits the synthesis of viral negative-strand RNA and viral budding. Furthermore, we also found that Ag_2S NCs activated the production of IFN-stimulating genes (ISGs) and the expression of proinflammation cytokines of Vero cells, which might inhibit the PEDV infection.

These inspiring findings offer experimental support for the further exploitation of Ag_2S NCs as a potential and highly effective antiviral agent *in vivo*. Given that SARS, MARS, and PEDV belong to the coronavirus family, our results suggest the possibility to develop efficient anti-SARS or anti-MARS reagents based on Ag_2S NCs or conjugation of Ag_2S NCs and functional molecules.

■ ASSOCIATED CONTENT

Supporting Information

The Supporting Information is available free of charge on the ACS Publications website at DOI: 10.1021/acsami.7b13811.

Cytotoxicity; plaque assay; Western blot; indirect immunofluorescence assay and primers sequence (PDF)

■ AUTHOR INFORMATION

Corresponding Authors

*E-mail: hyhan@mail.hzau.edu.cn (H.H.).
*E-mail: vet@mail.hzau.edu.cn (S.X.).

ORCID

Jiangong Liang: 0000-0002-8210-0210
Shaobo Xiao: 0000-0003-0023-9188
Heyou Han: 0000-0001-9406-0722

Notes

The authors declare no competing financial interest.

■ ACKNOWLEDGMENTS

We gratefully acknowledge the support for this research by the National Key R & D Program (2016YFD0500700), the National Natural Science Foundation of China (21778020, 21375043, and 31672569) and Sci-tech Innovation Foundation of Huazhong Agricultural University (2662017PY042).

■ REFERENCES

(1) Lin, Z.; Li, Y.; Guo, M.; Xu, T.; Wang, C.; Zhao, M.; Wang, H.; Chen, T.; Zhu, B. The Inhibition of H1N1 Influenza Virus-Induced Apoptosis by Silver Nanoparticles Functionalized with Zanamivir. *RSC Adv.* **2017**, *7*, 742−750.

(2) Rogers, J. V.; Parkinson, C. V.; Choi, Y. W.; Speshock, J. L.; Hussain, S. M. A Preliminary Assessment of Silver Nanoparticle Inhibition of Monkeypox Virus Plaque Formation. *Nanoscale Res. Lett.* **2008**, *3*, 129−133.

(3) Elechiguerra, J. L.; Burt, J. L.; Morones, J. R.; Camacho Bragado, A.; Gao, X.; Lara, H. H.; Yacaman, M. J. Interaction of Silver Nanoparticles with HIV-1. *J. Nanobiotechnol.* **2005**, *3*, 6−16.

(4) Papp, I.; Sieben, C.; Ludwig, K.; Roskamp, M.; Bottcher, C.; Schlecht, S.; Herrmann, A.; Haag, R. Inhibition of Influenza Virus Infection by Multivalent Sialic-Acid-Functionalized Gold Nanoparticles. *Small* **2010**, *6*, 2900−2906.

(5) Draz, M. S.; Wang, Y. J.; Chen, F. F.; Xu, Y.; Shafiee, H. Electrically Oscillating Plasmonic Nanoparticles for Enhanced DNA Vaccination Against Hepatitis C Virus. *Adv. Funct. Mater.* **2017**, *27*, 1604139−1604149.

(6) Barras, A.; Pagneux, Q.; Sane, F.; Wang, Q.; Boukherroub, R.; Hober, D.; Szunerits, S. High Efficiency of Functional Carbon Nanodots as Entry Inhibitors of Herpes Simplex Virus Type 1. *ACS Appl. Mater. Interfaces* **2016**, *8*, 9004−9013.

(7) Muñoz, A.; Sigwalt, D.; Illescas, B. M.; Luczkowiak, J.; Rodríguez-Pérez, L.; Nierengarten, I.; Holler, M.; Remy, J. S.; Buffet, K.; Vincent, S. P.; Rojo, J.; Delgado, R.; Nierengarten, J. F.; Martín, N. Synthesis of Giant Globular Multivalent Glycofullerenes as Potent Inhibitors in a Model of Ebola Virus Infection. *Nat. Chem.* **2016**, *8*, 50−57.

(8) Sametband, M.; Kalt, I.; Gedanken, A.; Sarid, R. Herpes Simplex Virus Type-1 Attachment Inhibition by Functionalized Graphene Oxide. *ACS Appl. Mater. Interfaces* **2014**, *6*, 1228−1235.

(9) Ziem, B.; Rahn, J.; Donskyi, I.; Silberreis, K.; Cuellar, L.; Dernedde, J.; Keil, G.; Mettenleiter, T. C.; Haag, R. Polyvalent 2D Entry Inhibitors for Pseudorabies and African Swine Fever Virus. *Macromol. Biosci.* **2017**, *17*, 1600499−1600508.

DOI: 10.1021/acsami.7b13811
ACS Appl. Mater. Interfaces XXXX, XXX, XXX−XXX

(10) Deokar, A. R.; Nagvenkar, A. P.; Kalt, I.; Shani, L.; Yeshurun, Y.; Gedanken, A.; Sarid, R. Graphene-Based "Hot Plate" for the Capture and Destruction of the Herpes Simplex Virus Type 1. *Bioconjugate Chem.* **2017**, *28*, 1115−1122.
(11) Wang, J.; Liu, Y.; Xu, K.; Qi, Y.; Zhong, J.; Zhang, K.; Li, J.; Wang, E.; Wu, Z.; Kang, Z. Broad-Spectrum Antiviral Property of Polyoxometalate Localized on a Cell Surface. *ACS Appl. Mater. Interfaces* **2014**, *6*, 9785−9789.
(12) Bhatia, S.; Lauster, D.; Bardua, M.; Ludwig, K.; Angioletti Uberti, S.; Popp, N.; Hoffmann, U.; Paulus, F.; Budt, M.; Stadtmuller, M.; Wolff, T.; Hamann, A.; Bottcher, C.; Herrmann, A.; Haag, R. Linear Polysialoside Outperforms Dendritic Analogs for Inhibition of Influenza Virus Infection in Vitro and in Vivo. *Biomaterials* **2017**, *138*, 22−34.
(13) Liang, J. J.; Wei, J. C.; Lee, Y. L.; Hsu, S. H.; Lin, J. J.; Lin, Y. L. Surfactant-Modified Nanoclay Exhibits an Antiviral Activity with High Potency and Broad Spectrum. *J. Virol.* **2014**, *88*, 4218−4228.
(14) Osminkina, L. A.; Timoshenko, V. Y.; Shilovsky, I. P.; Kornilaeva, G. V.; Shevchenko, S. N.; Gongalsky, M. B.; Tamarov, K. P.; Abramchuk, S. S.; Nikiforov, V. N.; Khaitov, M. R.; Karamov, E. V. Porous Silicon Nanoparticles as Scavengers of Hazardous Viruses. *J. Nanopart. Res.* **2014**, *16*, 2430−2440.
(15) Douglas, J. L.; Panis, M. L.; Ho, E.; Lin, K. Y.; Krawczyk, S. H.; Grant, D. M.; Cai, R.; Swaminathan, S.; Cihlar, T. Inhibition of Respiratory Syncytial Virus Fusion by the Small Molecule VP-14637 via Specific Interactions with F Protein. *J. Virol.* **2003**, *77*, 5054−5064.
(16) Yang, J.; Li, M.; Shen, X.; Liu, S. Influenza A Virus Entry Inhibitors Targeting the Hemagglutinin. *Viruses* **2013**, *5*, 352−373.
(17) Lauster, D.; Glanz, M.; Bardua, M.; Ludwig, K.; Hellmund, M.; Hoffmann, U.; Hamann, A.; Bottcher, C.; Haag, R.; Hackenberger, C. P. R.; Herrmann, A. Multivalent Peptide-Nanoparticle Conjugates for Influenza-Virus Inhibition. *Angew. Chem., Int. Ed.* **2017**, *56*, 5931−5936.
(18) Khanal, M.; Vausselin, T.; Barras, A.; Bande, O.; Turcheniuk, K.; Benazza, M.; Zaitsev, V.; Teodorescu, C. M.; Boukherroub, R.; Siriwardena, A.; Dubuisson, J.; Szunerits, S. Phenylboronic-Acid-Modified Nanoparticles: Potential Antiviral Therapeutics. *ACS Appl. Mater. Interfaces* **2013**, *5*, 12488−12498.
(19) Khanal, M.; Barras, A.; Vausselin, T.; Feneant, L.; Boukherroub, R.; Siriwardena, A.; Dubuisson, J.; Szunerits, S. Boronic Acid-Modified Lipid Nanocapsules: a Novel Platform for the Highly Efficient Inhibition of Hepatitis C Viral Entry. *Nanoscale* **2015**, *7*, 1392−1402.
(20) Yang, X. X.; Li, C. M.; Huang, C. Z. Curcumin Modified Silver Nanoparticles for Highly Efficient Inhibition of Respiratory Syncytial Virus Infection. *Nanoscale* **2016**, *8*, 3040−3048.
(21) Ye, S.; Shao, K.; Li, Z.; Guo, N.; Zuo, Y.; Li, Q.; Lu, Z.; Chen, L.; He, Q.; Han, H. Antiviral Activity of Graphene Oxide: How Sharp Edged Structure and Charge Matter. *ACS Appl. Mater. Interfaces* **2015**, *7*, 21571−21579.
(22) Wang, D.; Fang, L.; Shi, Y.; Zhang, H.; Gao, L.; Peng, G.; Chen, H.; Li, K.; Xiao, S. Porcine Epidemic Diarrhea Virus 3C-Like Protease Regulates its Interferon Antagonism by Cleaving NEMO. *J. Virol.* **2016**, *90*, 2090−2101.
(23) Ding, Z.; Fang, L.; Jing, H.; Zeng, S.; Wang, D.; Liu, L.; Zhang, H.; Luo, R.; Chen, H.; Xiao, S. Porcine Epidemic Diarrhea Virus Nucleocapsid Protein Antagonizes Beta Interferon Production by Sequestering the Interaction between IRF3 and TBK1. *J. Virol.* **2014**, *88*, 8936−8945.
(24) Du, Y.; Xu, B.; Fu, T.; Cai, M.; Li, F.; Zhang, Y.; Wang, Q. Near-Infrared Photoluminescent Ag_2S Quantum Dots from a Single Source Precursor. *J. Am. Chem. Soc.* **2010**, *132*, 1470−1471.
(25) Gui, R.; Wan, A.; Liu, X.; Yuan, W.; Jin, H. Water-Soluble Multidentate Polymers Compactly Coating Ag_2S Quantum Dots with Minimized Hydrodynamic Size and Bright Emission Tunable from Red to Second Near-Infrared Region. *Nanoscale* **2014**, *6*, 5467−5473.
(26) Zhang, Y.; Hong, G.; Zhang, Y.; Chen, G.; Li, F.; Dai, H.; Wang, Q. Ag_2S Quantum Dot: a Bright and Biocompatible Fluorescent Nanoprobe in the Second Near-Infrared Window. *ACS Nano* **2012**, *6*, 3695−3702.
(27) Tan, L.; Wan, A.; Li, H. Conjugating S-nitrosothiols with Glutathiose Stabilized Silver Sulfide Quantum Dots for Controlled Nitric Oxide Release and Near-Infrared Fluorescence Imaging. *ACS Appl. Mater. Interfaces* **2013**, *5*, 11163−11171.
(28) Tang, R.; Xue, J.; Xu, B.; Shen, D.; Sudlow, G. P.; Achilefu, S. Tunable Ultrasmall Visible-to-Extended Near-Infrared Emitting Silver Sulfide Quantum Dots for Integrin-Targeted Cancer Imaging. *ACS Nano* **2015**, *9*, 220−230.
(29) Yang, T.; Tang, Y.; Liu, L.; Lv, X.; Wang, Q.; Ke, H.; Deng, Y.; Yang, H.; Yang, X.; Liu, G.; Zhao, Y.; Chen, H. Size-Dependent Ag_2S Nanodots for Second Near-Infrared Fluorescence/Photoacoustics Imaging and Simultaneous Photothermal Therapy. *ACS Nano* **2017**, *11*, 1848−1857.
(30) Miao, P.; Tang, Y.; Wang, B.; Meng, F. Near-Infrared Ag_2S Quantum Dots-Based DNA Logic Gate Platform for miRNA Diagnostics. *Anal. Chem.* **2016**, *88*, 7567−7573.
(31) Wang, C.; Wang, Y.; Xu, L.; Zhang, D.; Liu, M.; Li, X.; Sun, H.; Lin, Q.; Yang, B. Facile Aqueous-Phase Synthesis of Biocompatible and Fluorescent Ag_2S Nanoclusters for Bioimaging: Tunable Photoluminescence from Red to Near Infrared. *Small* **2012**, *8*, 3137−3142.
(32) Liu, A. A.; Zhang, Z.; Sun, E. Z.; Zheng, Z.; Zhang, Z. L.; Hu, Q.; Wang, H.; Pang, D. W. Simultaneous Visualization of Parental and Progeny Viruses by a Capsid-Specific Halo Tag Labeling Strategy. *ACS Nano* **2016**, *10*, 1147−1155.
(33) Huang, B. H.; Lin, Y.; Zhang, Z. L.; Zhuan, F.; Liu, A. A.; Xie, M.; Tian, Z. Q.; Zhang, Z.; Wang, H.; Pang, D. W. Surface Labeling of Enveloped Viruses Assisted by Host Cells. *ACS Chem. Biol.* **2012**, *7*, 683−688.
(34) Luo, R.; Fang, L.; Jin, H.; Jiang, Y.; Wang, D.; Chen, H.; Xiao, S. Antiviral Activity of Type I and Type III Interferons Against Porcine Reproductive and Respiratory Syndrome Virus (PRRSV). *Antiviral Res.* **2011**, *91*, 99−101.
(35) Alvarez, A. L.; Melon, S.; Dalton, K. P.; Nicieza, I.; Roque, A.; Suarez, B.; Parra, F. Apple Pomace, a by-Product From the Asturian Cider Industry, Inhibits Herpes Simplex Virus Types 1 and 2 in Vitro Replication: Study of its Mechanisms of Action. *J. Med. Food* **2012**, *15*, 581−587.
(36) Gescher, K.; Hensel, A.; Hafezi, W.; Derksen, A.; Kuhn, J. Oligomeric Proanthocyanidins from Rumex Acetosa L. Inhibit the Attachment of Herpes Simplex Virus Type-1. *Antiviral Res.* **2011**, *89*, 9−18.
(37) Duan, E.; Wang, D.; Fang, L.; Ma, J.; Luo, J.; Chen, H.; Li, K.; Xiao, S. Suppression of Porcine Reproductive and Respiratory Syndrome Virus Proliferation by Glycyrrhizin. *Antiviral Res.* **2015**, *120*, 122−125.
(38) Wang, Y.; Yan, X. P. Fabrication of Vascular Endothelial Growth Factor Antibody Bioconjugated Ultrasmall Near-Infrared Fluorescent Ag_2S Quantum Dots for Targeted Cancer Imaging in Vivo. *Chem. Commun.* **2013**, *49*, 3324−3326.
(39) Xu, X.; Zhang, H.; Zhang, Q.; Huang, Y.; Dong, J.; Liang, Y.; Liu, H. J.; Tong, D. Porcine Epidemic Diarrhea Virus N Protein Prolongs S-Phase Cell Cycle, Induces Endoplasmic Reticulum Stress, and Up-Regulates Interleukin-8 Expression. *Vet. Microbiol.* **2013**, *164*, 212−221.
(40) Winnik, F. M.; Maysinger, D. Quantum Dot Cytotoxicity and Ways to Reduce it. *Acc. Chem. Res.* **2013**, *46*, 672−680.
(41) van Kan-Davelaar, H. E.; van Hest, J. C. M.; Cornelissen, J. J. L. M.; Koay, M. S. T. Using Viruses as Nanomedicines. *Br. J. Pharmacol.* **2014**, *171*, 4001−4009.
(42) Du, T.; Cai, K.; Han, H.; Fang, L.; Liang, J.; Xiao, S. Probing the Interactions of CdTe Quantum Dots with Pseudorabies Virus. *Sci. Rep.* **2015**, *5*, 16403.
(43) Hao, J.; Huang, L. L.; Zhang, R.; Wang, H. Z.; Xie, H. Y. A Mild and Reliable Method to Label Enveloped Virus with Quantum Dots by Copper-Free Click Chemistry. *Anal. Chem.* **2012**, *84*, 8364−8370.
(44) Zhang, P.; Liu, S.; Gao, D.; Hu, D.; Gong, P.; Sheng, Z.; Deng, J.; Ma, Y.; Cai, L. Click-Functionalized Compact Quantum Dots Protected by Multidentate-Imidazole Ligands: Conjugation-Ready Nanotags for Living-Virus Labeling and Imaging. *J. Am. Chem. Soc.* **2012**, *134*, 8388−8391.
(45) Baram-Pinto, D.; Shukla, S.; Perkas, N.; Gedanken, A.; Sarid, R. Inhibition of Herpes Simplex Virus Type 1 Infection by Silver

DOI: 10.1021/acsami.7b13811
ACS Appl. Mater. Interfaces XXXX, XXX, XXX−XXX

Nanoparticles Capped with Mercaptoethane Sulfonate. *Bioconjugate Chem.* **2009**, *20*, 1497−1502.
(46) Fensterl, V.; Sen, G. C. Interferon-Induced I Fit Proteins: Their Role in Viral Pathogenesis. *J. Virol.* **2015**, *89*, 2462−2468.
(47) Schoggins, J. W.; Wilson, S. J.; Panis, M.; Murphy, M. Y.; Jones, C. T.; Bieniasz, P.; Rice, C. M. A Diverse Range of Gene Products are Effectors of the Type I Interferon Antiviral Response. *Nature* **2011**, *472*, 481−485.
(48) Tokumoto, Y.; Hiasa, Y.; Uesugi, K.; Watanabe, T.; Mashiba, T.; Abe, M.; Kumagi, T.; Ikeda, Y.; Matsuura, B.; Onji, M. Ribavirin Regulates Hepatitis C Virus Replication through Enhancing Interferon-Stimulated Genes and Interleukin 8. *J. Infect. Dis.* **2012**, *205*, 1121−1130.
(49) Yu, Y.; Huang, X.; Liu, J.; Zhang, J.; Hu, Y.; Yang, Y.; Huang, Y.; Qin, Q. Fish TRIM32 Functions as a Critical Antiviral Molecule Against Iridovirus and Nodavirus. *Fish Shellfish Immunol.* **2017**, *60*, 33−43.
(50) Schoggins, J. W.; Rice, C. M. Interferon-Stimulated Genes and their Antiviral Effector Functions. *Curr. Opin. Virol.* **2011**, *1*, 519−525.
(51) Imaizumi, T.; Yoshida, H.; Hayakari, R.; Xing, F.; Wang, L.; Matsumiya, T.; Tanji, K.; Kawaguchi, S.; Murakami, M.; Tanaka, H. Interferon-Stimulated Gene (ISG) 60, as well as ISG56 and ISG54, Positively Regulates TLR3/IFN-beta/STAT1 Axis in U373MG Human Astrocytoma Cells. *Neurosci. Res.* **2016**, *105*, 35−41.
(52) Reich, N. C. A Death-Promoting Role for ISG54/IFIT2. *J. Interferon Cytokine Res.* **2013**, *33*, 199−205.
(53) Von Itzstein, M. The War Against Influenza: Discovery and Development of Sialidase Inhibitors. *Nat. Rev. Drug Discovery* **2007**, *6*, 967−974.
(54) Tayyari, F.; Marchant, D.; Moraes, T. J.; Duan, W.; Mastrangelo, P.; Hegele, R. G. Identification of Nucleolin as a Cellular Receptor for Human Respiratory Syncytial Virus. *Nat. Med.* **2011**, *17*, 1132−1135.
(55) Galdiero, S.; Falanga, A.; Vitiello, M.; Cantisani, M.; Marra, V.; Galdiero, M. Silver Nanoparticles as Potential Antiviral Agents. *Molecules* **2011**, *16*, 8894−8918.
(56) Li, C. M.; Zheng, L. L.; Yang, X. X.; Wan, X. Y.; Wu, W. B.; Zhen, S. J.; Li, Y. F.; Luo, L. F.; Huang, C. Z. DNA-AuNP Networks on Cell Membranes as a Protective Barrier to Inhibit Viral Attachment, Entry and Budding. *Biomaterials* **2016**, *77*, 216−226.
(57) Baram-Pinto, D.; Shukla, S.; Gedanken, A.; Sarid, R. Inhibition of HSV-1 Attachment, Entry, and Cell-to-Cell Spread by Functionalized Multivalent Gold Nanoparticles. *Small* **2010**, *6*, 1044−1050.
(58) Khandelwal, N.; Kaur, G.; Kumar, N.; Tiwari, A. Application of Silver Nanoparticles in Viral Inhibition: A New Hope for Antivirals. *Dig. J. Nanomater. Bios.* **2014**, *9*, 175−186.
(59) Dostalova, S.; Moulick, A.; Milosavljevic, V.; Guran, R.; Kominkova, M.; Cihalova, K.; Heger, Z.; Blazkova, L.; Kopel, P.; Hynek, D.; Vaculovicova, M.; Adam, V.; Kizek, R. Antiviral Activity of Fullerene C60 Nanocrystals Modified with Derivatives of Anionic Antimicrobial Peptide Maximin H5. *Monatsh. Chem.* **2016**, *147*, 905−918.
(60) De Souza, E. S. J. M.; Hanchuk, T. D.; Santos, M. I.; Kobarg, J.; Bajgelman, M. C.; Cardoso, M. B. Viral Inhibition Mechanism Mediated by Surface-Modified Silica Nanoparticles. *ACS Appl. Mater. Interfaces* **2016**, *8*, 16564−16572.
(61) Lisov, A.; Vrublevskaya, V.; Lisova, Z.; Leontievsky, A.; Morenkov, O. A 2,5-Dihydroxybenzoic Acid-Gelatin Conjugate: The Synthesis, Antiviral Activity and Mechanism of Antiviral Action Against Two Alphaherpesviruses. *Viruses* **2015**, *7*, 5343−5360.
(62) Tarr, A. W.; Lafaye, P.; Meredith, L.; Damier-Piolle, L.; Urbanowicz, R. A.; Meola, A.; Jestin, J. L.; Brown, R. J.; McKeating, J. A.; Rey, F. A.; Ball, J. K.; Krey, T. An Alpaca Nanobody Inhibits Hepatitis C Virus Entry and Cell-to-Cell Transmission. *Hepatology* **2013**, *58*, 932−939.
(63) Sun, R. W. Y.; Chen, R.; Chung, N. P. Y.; Ho, C. M.; Lin, C. L. S.; Che, C. M. Silver Nanoparticles Fabricated in Hepes Buffer Exhibit Cytoprotective Activities toward HIV-1 Infected Cells. *Chem. Commun.* **2005**, *40*, 5059−5061.
(64) Orlowski, P.; Tomaszewska, E.; Gniadek, M.; Baska, P.; Nowakowska, J.; Sokolowska, J.; Nowak, Z.; Donten, M.; Celichowski, G.; Grobelny, J.; Krzyzowska, M. Tannic Acid Modified Silver Nanoparticles Show Antiviral Activity in Herpes Simplex Virus Type 2 Infection. *PLoS One* **2014**, *9*, e104113.
(65) Lee, E. C.; Davis-Poynter, N.; Nguyen, C. T.; Peters, A. A.; Monteith, G. R.; Strounina, E.; Popat, A.; Ross, B. P. GAG Mimetic Functionalised Solid and Mesoporous Silica nanoparticles as Viral Entry Inhibitors of Herpes Simplex Type 1 and Type 2 Viruses. *Nanoscale* **2016**, *8*, 16192−16196.
(66) Yang, X. X.; Li, C. M.; Li, Y. F.; Wang, J.; Huang, C. Z. Synergistic Antiviral Effect of Curcumin Functionalized Graphene Oxide against Respiratory Syncytial Virus Infection. *Nanoscale* **2017**, *9*, 16086−16092.
(67) Li, Y.; Lin, Z.; Zhao, M.; Xu, T.; Wang, C.; Hua, L.; Wang, H.; Xia, H.; Zhu, B. Silver Nanoparticle Based Codelivery of Oseltamivir to Inhibit the Activity of the H1N1 Influenza Virus through ROS-Mediated Signaling Pathways. *ACS Appl. Mater. Interfaces* **2016**, *8*, 24385−24393.
(68) Du, T.; Liang, J.; Dong, N.; Liu, L.; Fang, L.; Xiao, S.; Han, H. Carbon Dots as Inhibitors of Virus by Activation of Type I Interferon Response. *Carbon* **2016**, *110*, 278−285.

DOI: 10.1021/acsami.7b13811
ACS Appl. Mater. Interfaces XXXX, XXX, XXX−XXX